Electronic Supplementary Material (ESI) for Journal of Materials Chemistry C.
This journal is © The Royal Society of Chemistry 2022

# Supporting Information for

## 1D Cu(I)-I-pyrazine coordination polymer with pressure-induced phase transition and opto-electronic response à la carte depending on mechanical stimuli, temperature and CuI content.

María Murillo [a], Javier Alvarez-Conde[b], Reinhold Wannemacher[b], Juan Cabanillas-Gonzalez[b], Javier González-Platas[C], Ulises R. Rodríguez-Mendoza[d], Akun Liang[e], Robin Turnbull[e], Daniel Errandonea[e], Jose Ignacio Martinez[f], and Pilar Amo-Ochoa[a,g]*

## Contents

## S1. Synthesis and Characterization

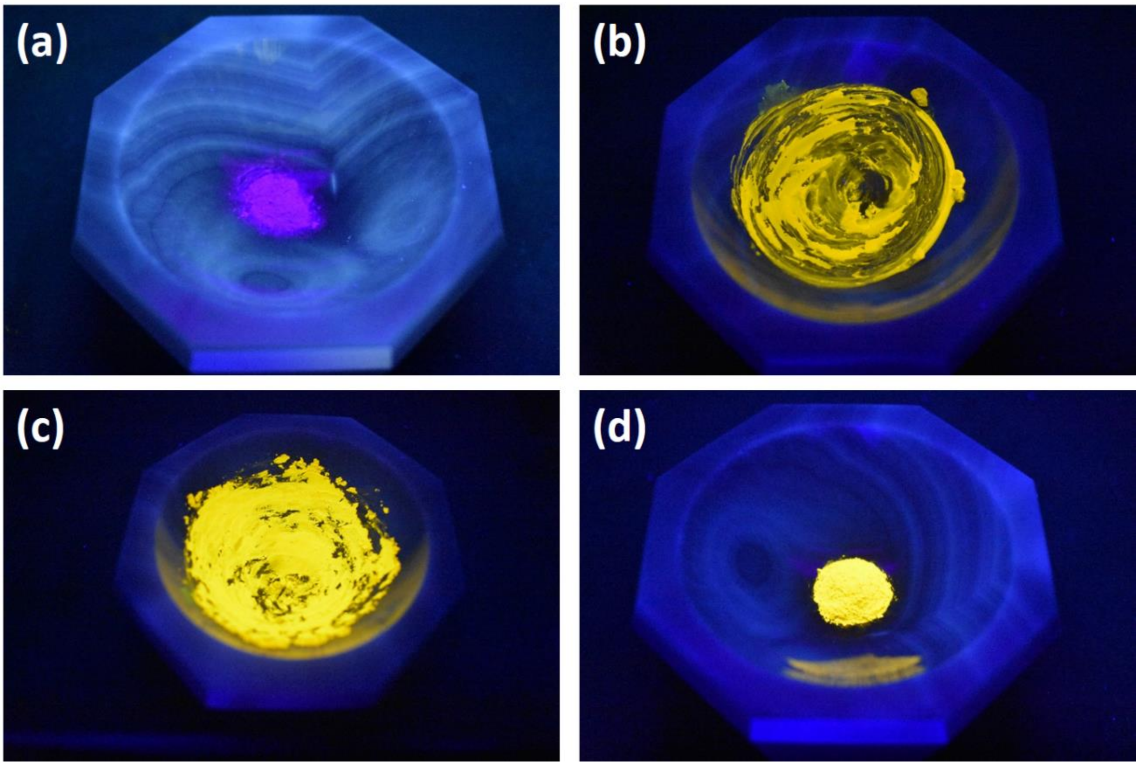

**Figure S1.** Solvent free mechano synthesis by grinding of **1D-[CuI(PyzBr)]$_n$** polycrystals under UV light ($\lambda_{exc}$ = 365 nm). CuI **(a)**, CuI + 2-bromopyrazine **(b)**, CuI + 2-bromopyrazine after grinding for 2 minutes to ensure the formation of the CP **(c)** and **1D-[CuI(PyzBr)]$_n$** polycrystals **(d)**.

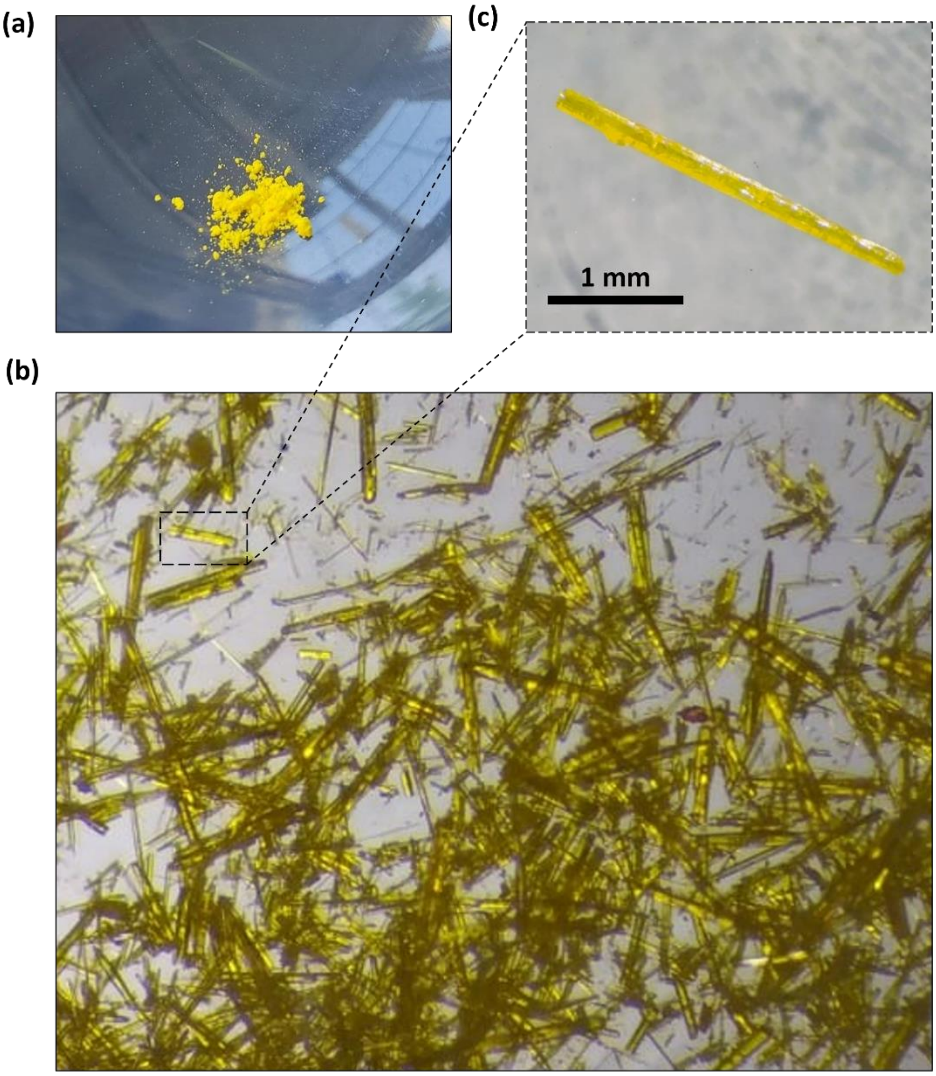

**Figure S2.** Polycrystalline powder of **1D-[CuI(PyzBr)]$_n$** (**a**), single crystals obtained by recrystallization in acetonitrile (**b**), and microscope image of **1D-[CuI(PyzBr)]$_n$** single crystal (**c**).

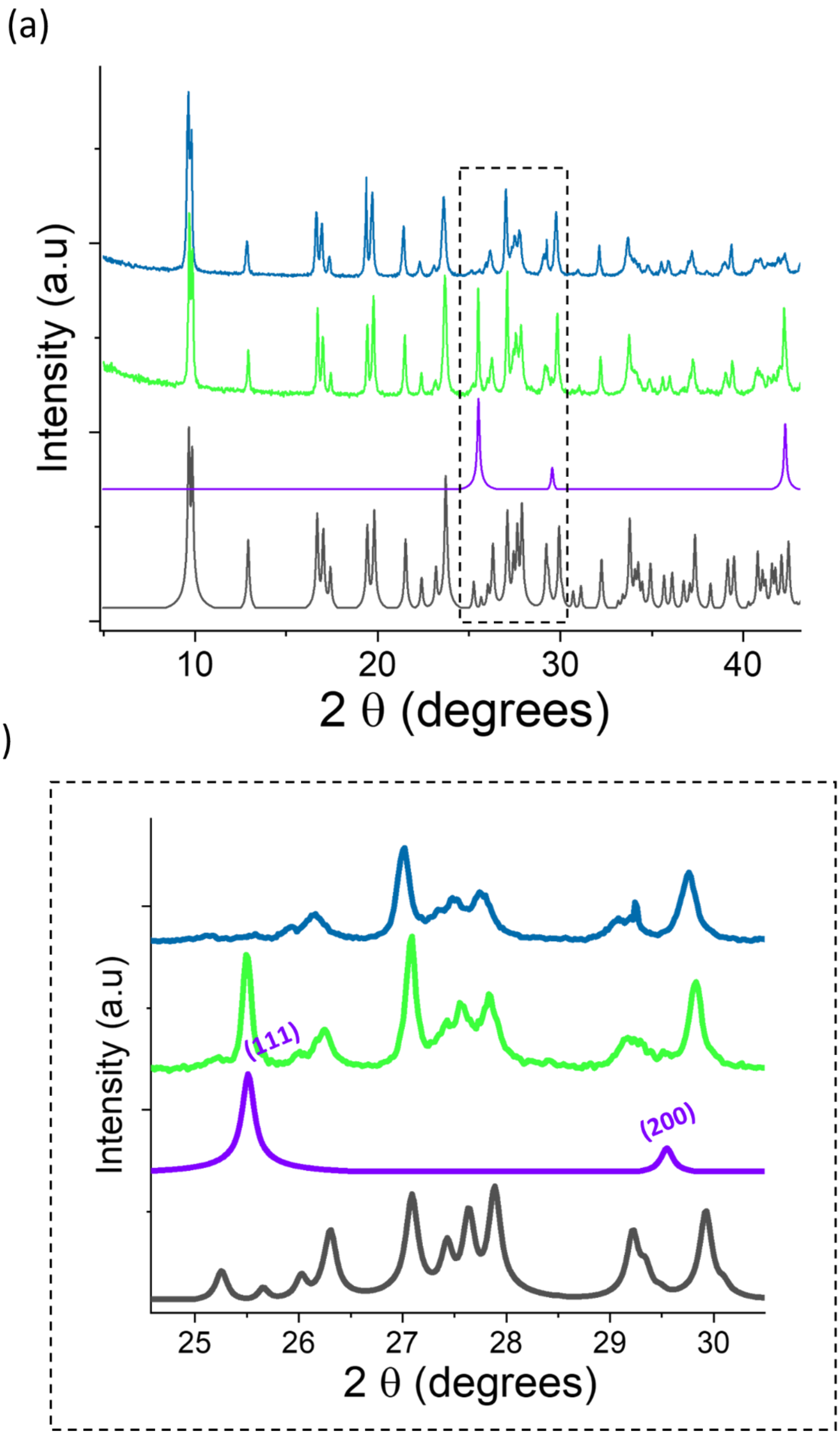

**Figure S3.** X-ray powder diffractograms (PXRD) of **[CuI(PyzBr)]$_n$** (**a**): Theoretical (black line), copper iodide (violet line), experimental polycrystalline **[CuI(PyzBr)]$_n$** obtained by mechanical solvent-free synthesis with a % of CuI (green line) and **[CuI(PyzBr)]$_n$** single crystals obtained by recrystallization (blue line).

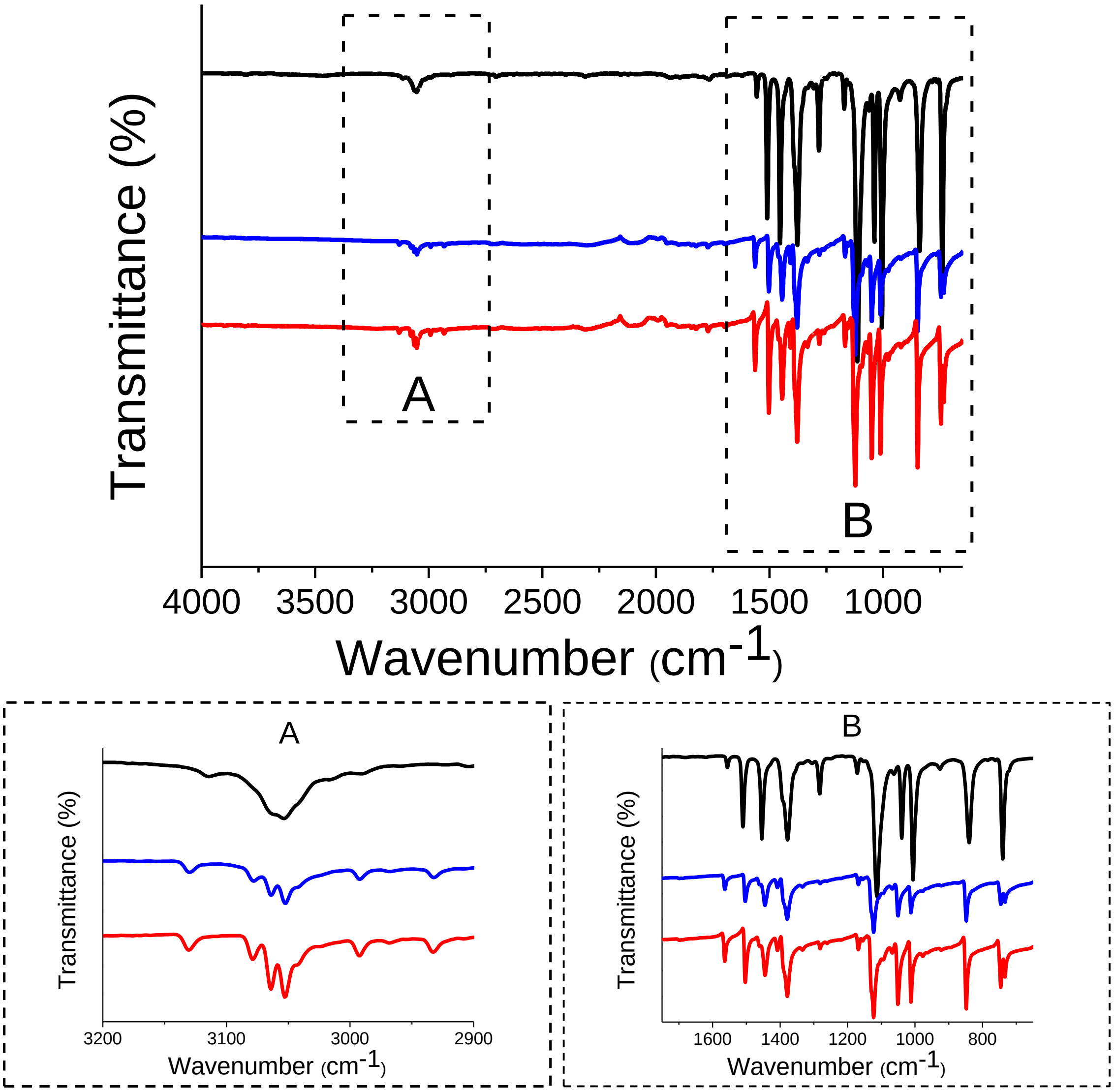

**Figure S4.** IR Spectra of 2-Bromo pyrazine **(PyzBr)** (black line), **$[CuI(PyzBr)]_n$** single crystal (blue line) and powder (**$[CuI(PyzBr)]_n$ polycrystals)** (red line). Boxed figures: Expansion of the wavenumber zone between 3200-2900 cm$^{-1}$ (A) and 1750-650 cm$^{-1}$ (B).

## S2. Thermogravimetric analysis (TGA)

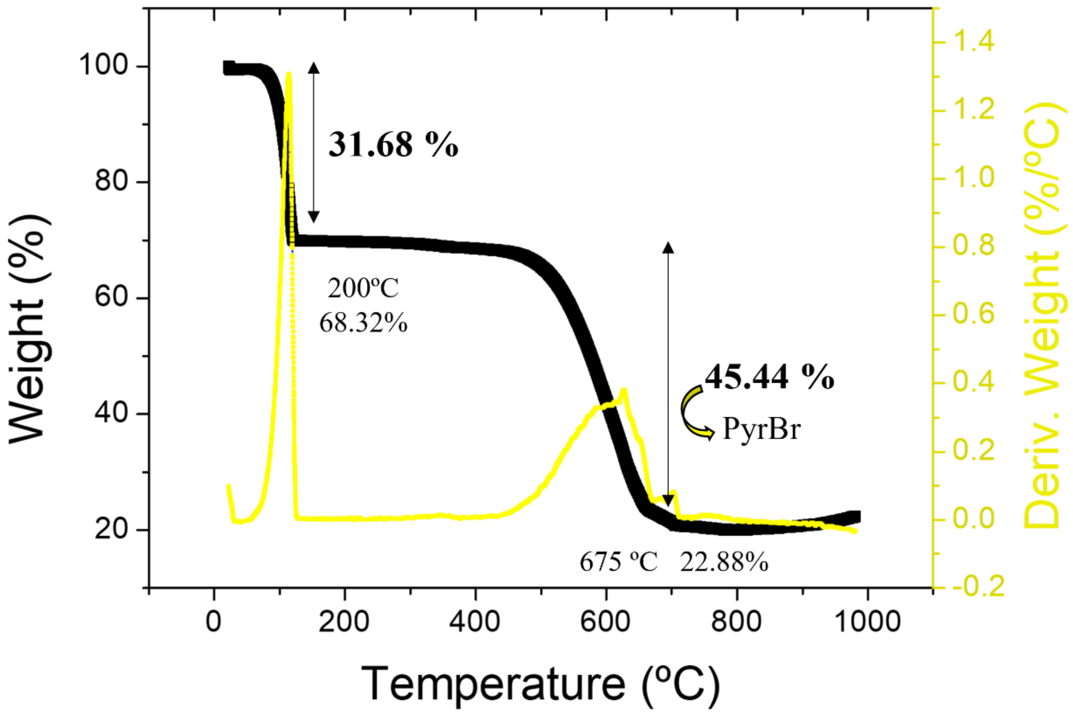

**Figure S5.** Thermogravimetric analysis of **1D-[CuI(PyzBr)]$_n$** polycrystals under nitrogen gas with flow rate 90 mL/min and heating rate 10 ºC/min.

**Table S1.** Decomposition temperatures, maximum loss, and residual weights of **1D-[CuI(PyzBr)]$_n$** polycrystals

| Coordination polymer | T$_{max}$ (°C) | D$_{max}$ (%/°C) | W$_R$ (%) |
|---|---|---|---|
| 1D-[CuI(PyzBr)]$_n$ | 114 | 1.32 | 22.88 |

## S3. Structure Determination

**Table S2.** Lattice parameters of compound **1D-[CuI(PyzBr)]$_n$.**

| **Compound** | **1D-[CuI(PyzBr)]$_n$** | |
|---|---|---|
| | 250 K | 100 K |
| Empirical formula | $C_4H_3BrCuIN_2$ | $C_4H_3BrCuIN_2$ |
| Formula weight | 349.43 | 349.43 |
| T (K) | 250(2) | 100(2) |
| λ (Å) | 0.71073 | |
| Crystal system | Orthorhombic | Orthorhombic |
| Space group | $P\,2_1\,2_1\,2_1$ | $P\,2_1\,2_1\,2_1$ |
| a (Å) | 4.10580(10) | 4.07790(10) |
| b (Å) | 10.5968(3) | 10.5973(2) |
| c (Å) | 17.8843(6) | 17.6896(4) |
| α (°) | 90 | 90 |
| β (°) | 90 | 90 |
| γ (°) | 90 | 90 |
| V (Å$^3$) | 778.12(4) | 764.45(3) |
| Z | 4 | 4 |
| $\rho_{calc}$ (g·cm$^{-3}$) | 2.983 | 3.036 |
| μ (mm$^{-1}$) | 11.822 | 12.033 |
| F (000) | 632 | 632 |
| Reflections collected | 9949 | 5084 |
| Unique data/parameters | 1410/82 | 1566/82 |
| Goodness of fit (S) | 1.027 | 1.074 |
| *R1/wR2* [$I>2\sigma(I)$] | 0.0207/0.0605 | 0.0182/0.0352 |
| *R1/wR2* [all data] | 0.0268/0.0953 | 0.0197/0.0358 |
| Largest diffraction peak and hole (e Å$^{-3}$) | 0.872/-1.220 | 0.49/-0.59 |

**Table S3.** Bond distances and angles of compound **1D-[CuI(PyzBr)]$_n$**.

| Distances | 1D-[CuI(PyzBr)]$_n$ | |
|---|---|---|
| | **250 K** | **100 K** |
| Cu-I1$_{rail}$ | 2.6298(9) | 2.6227(7) |
| Cu-I1$^{i}_{rail}$ | 2.6455(9) | 2.6498(7) |
| Δ[Cu-I1$_{rail}$] | 0.0157 | 0.0271 |
| Cu-I1$_{rung}$ | 2.6224(8) | 2.6210(6) |
| Cu-N1 | 2.053(5) | 2.053(4) |
| Cu-Cu$^{i}$ | 2.7967(11) | 2.7674(9) |
| Cu-Cu$^{ii}$ | 2.7967(11) | 2.7674(9) |
| Δ[Cu-Cu] | 0.000 | 0.000 |
| I1-Cu1-I1$^{i}$ | 115.49(3) | 116.00(3) |
| I1-Cu1-I1$^{ii}$ | 116.04(3) | 116.95 (3) |
| I1$^{i}$-Cu1-I1$^{ii}$ | 102.21(2) | 101.32(2) |
| Cu1-I1-Cu1$^{i}$ | 64.35(2) | 63.71(2) |
| Cu1-I1-Cu1$^{ii}$ | 64.13(2) | 63.34(2) |
| Cu1$^{i}$-I1-Cu1$^{ii}$ | 102.21(2) | 101.32(2) |
| I1$^{i}$-Cu1-I1-Cu1$^{ii}$ | -119.83(3) | 119.12(3) |

(i): -1/2+x, 3/2-y,1-z; (ii): ½+x,3/2-y,1-z (for 250K)
(i): -1/2+x, 7/2-y, -z; (ii): ½+x, 7/2-y,-z (for 100K)

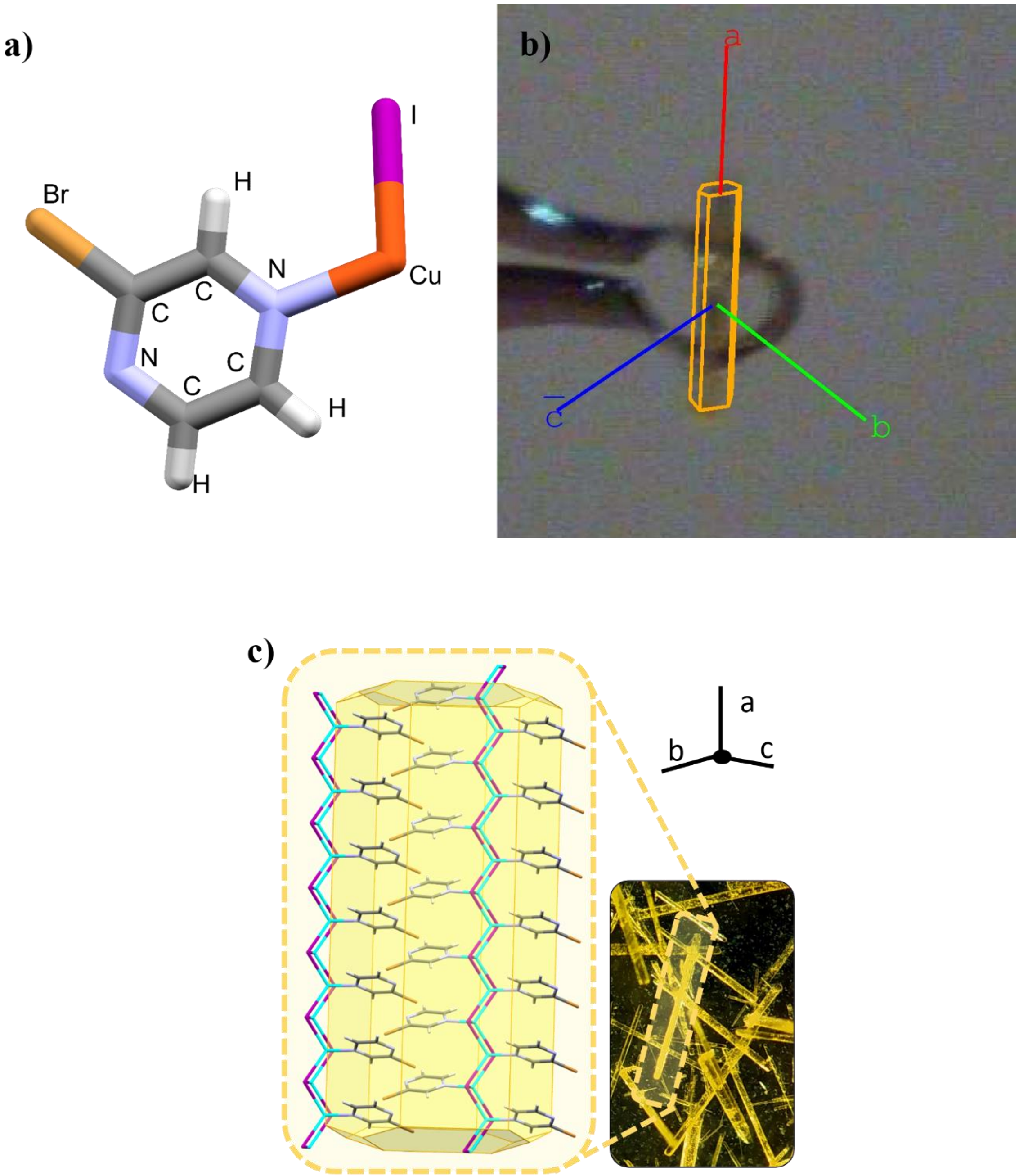

**Figure S6.** Mercury Cambridge Crystallographic Data Centre (CCDC) representation of [CuI(PyzBr)]$_n$ unit cell with atom labels (**a**), single crystal indexation (**b**), and semi-empirical theoretical calculations of morphology using Molecular Orbital PACkage (MOPAC) (**c**).

## S4. Quasi- hydrostatic pressure X-ray diffraction studies.

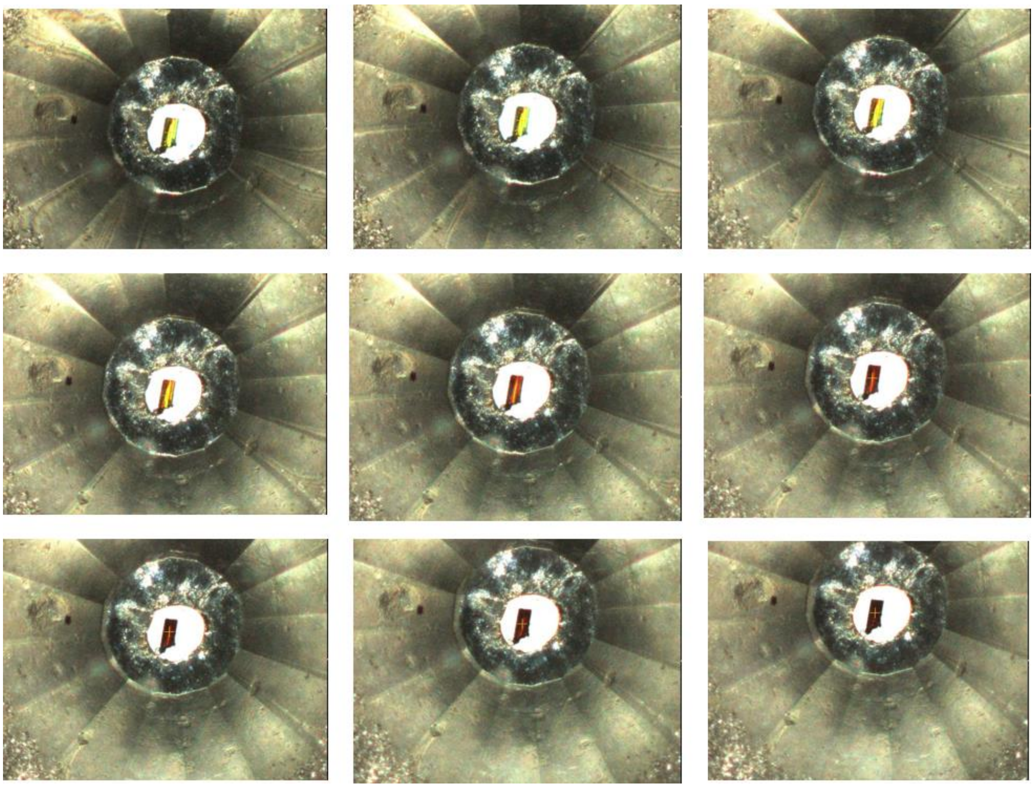

**Figure S7.** Single crystal of [CuI(**PyzBr**)]n in diamond anvil cell under pressure, from 0 GPa to 3.7 GPa.

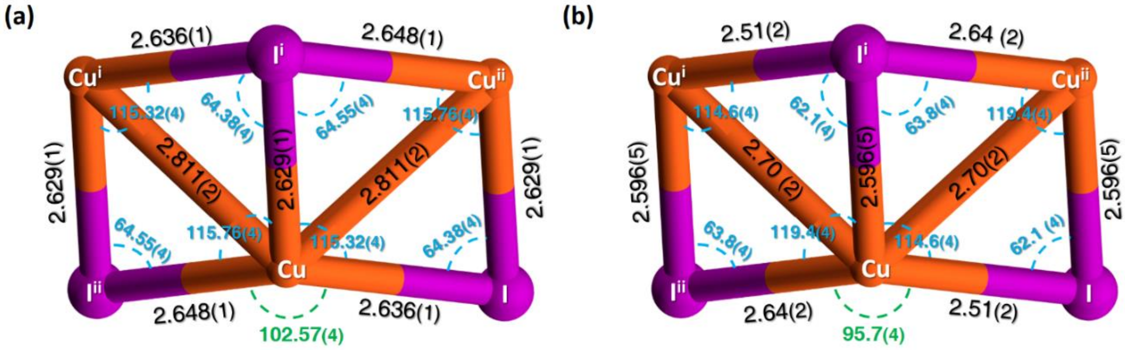

**Figure S8.** Cu-I chains with atoms labelled, distances (black) and angles (blue) for [CuI(PyzBr)]n at 298 K and applied pressure of 0 GPa (**a**) and at 3.76 GPa (**b**)

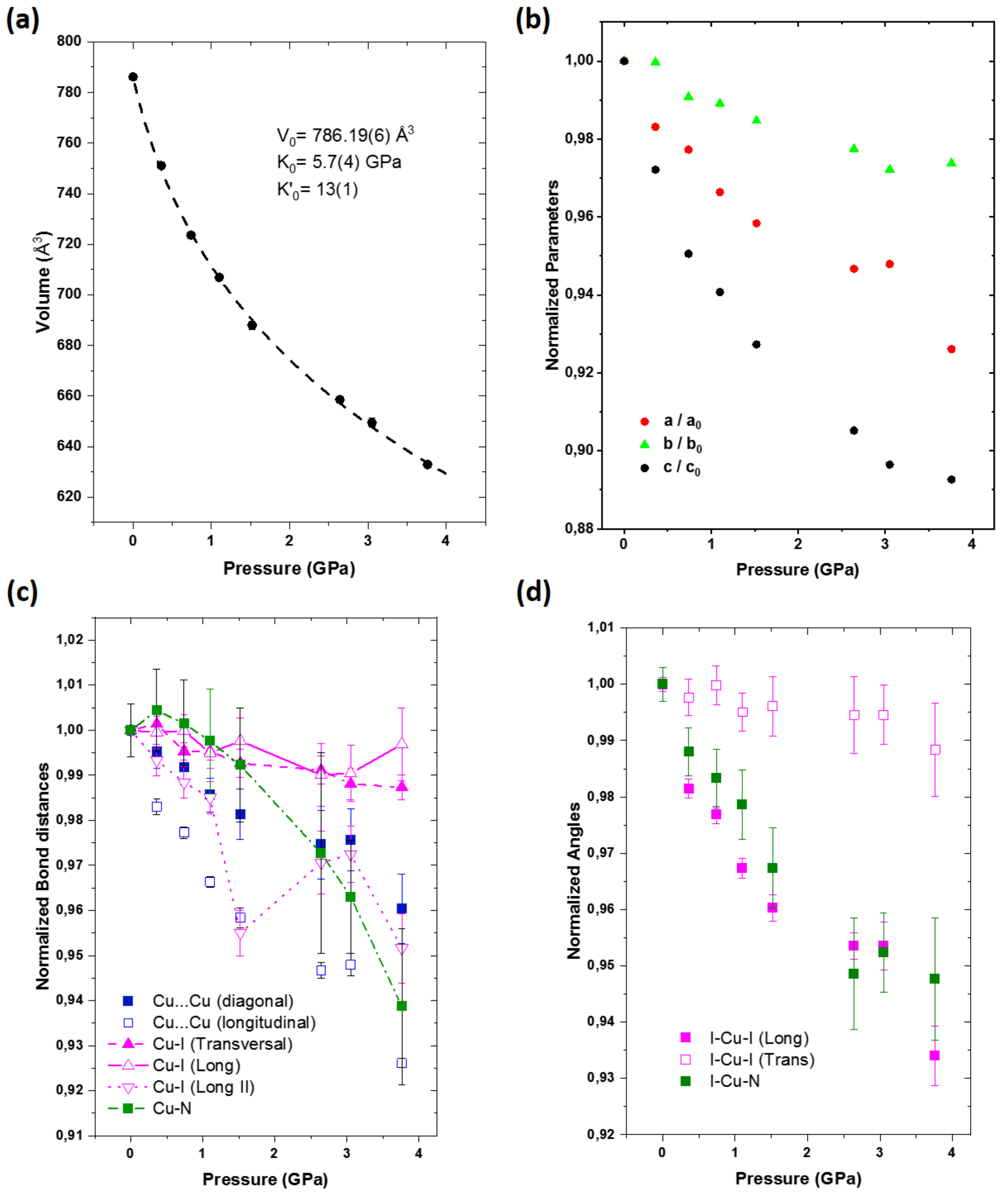

**Figure S9.** Normalized parameters for **[CuI(PyzBr)]$_n$** Dashed lines correspond to the respective EoS model fit (**a** and **b**).Variation of the Cu···Cu, Cu-N and Cu-I distances (**c**) and angles (**d**) with pressure. Error bars represent the standard for each value.

## S5. Temperature dependent photoluminescence (PL)

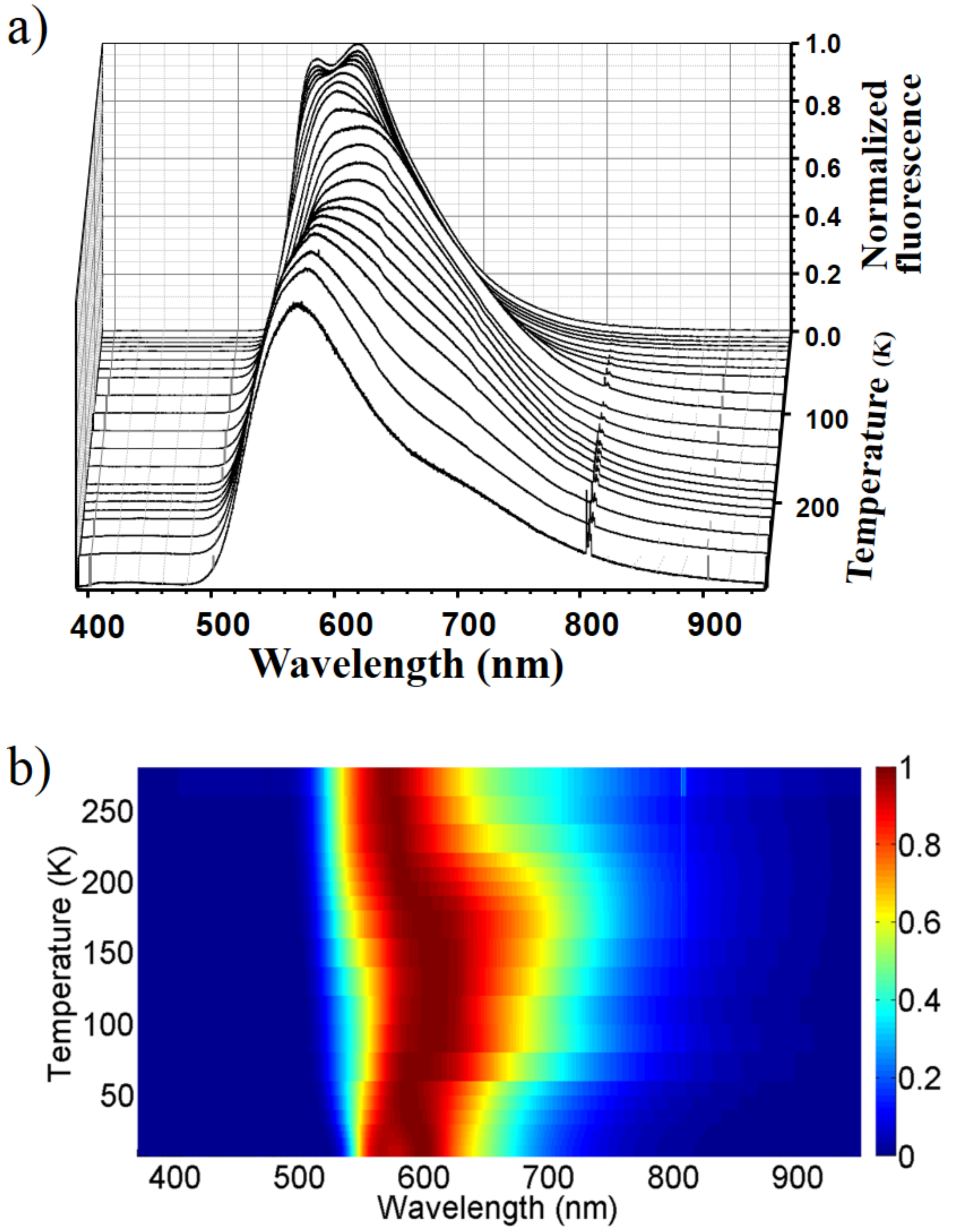

**Figure S10.** 3D **(a)** and 2D **(b)** Temperature dependence of normalized photoluminescence spectra in the solid-state ($\lambda_{exc}$ = 355 nm) for **1D-[CuI(PyzBr)]$_n$** polycrystals.

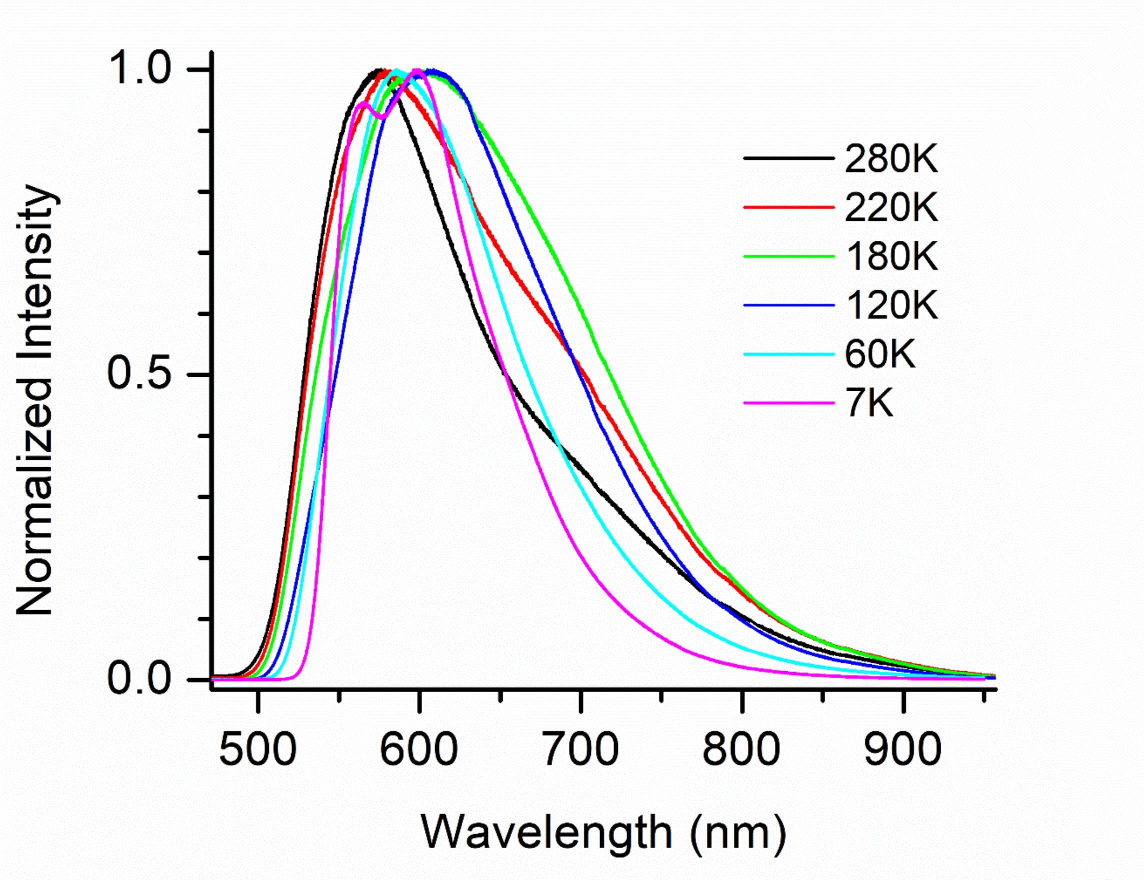

**Figure S11.** Normalized PL for this **[CuI(PyzBr)]n** polycrystalline powder at selected temperatures

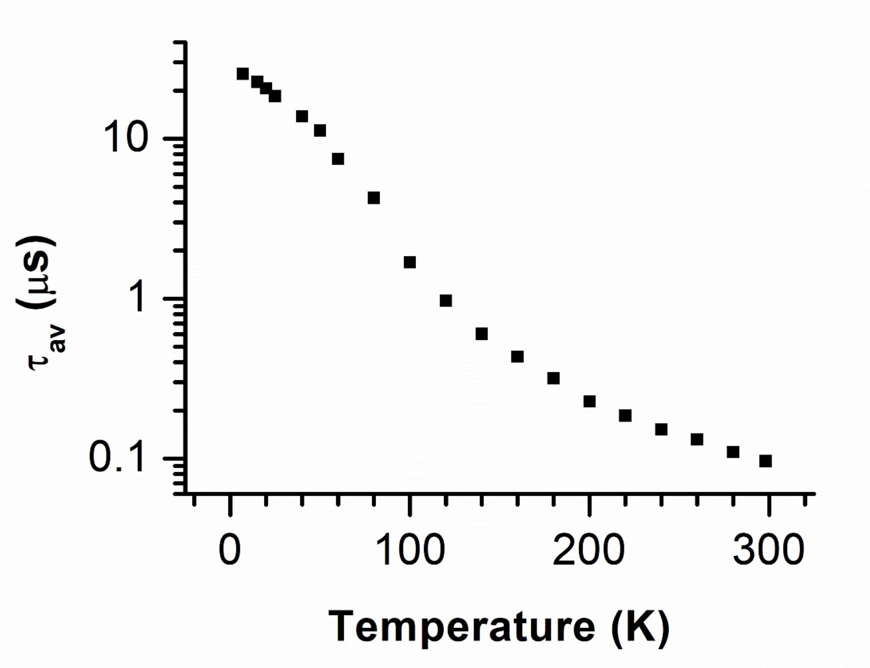

**Figure S12.** Temperature dependence of the intensity-averaged lifetime of $[CuI(PyzBr)]_n$ polycrystals. Excitation wavelength 355 nm, detection wavelength 570 nm.

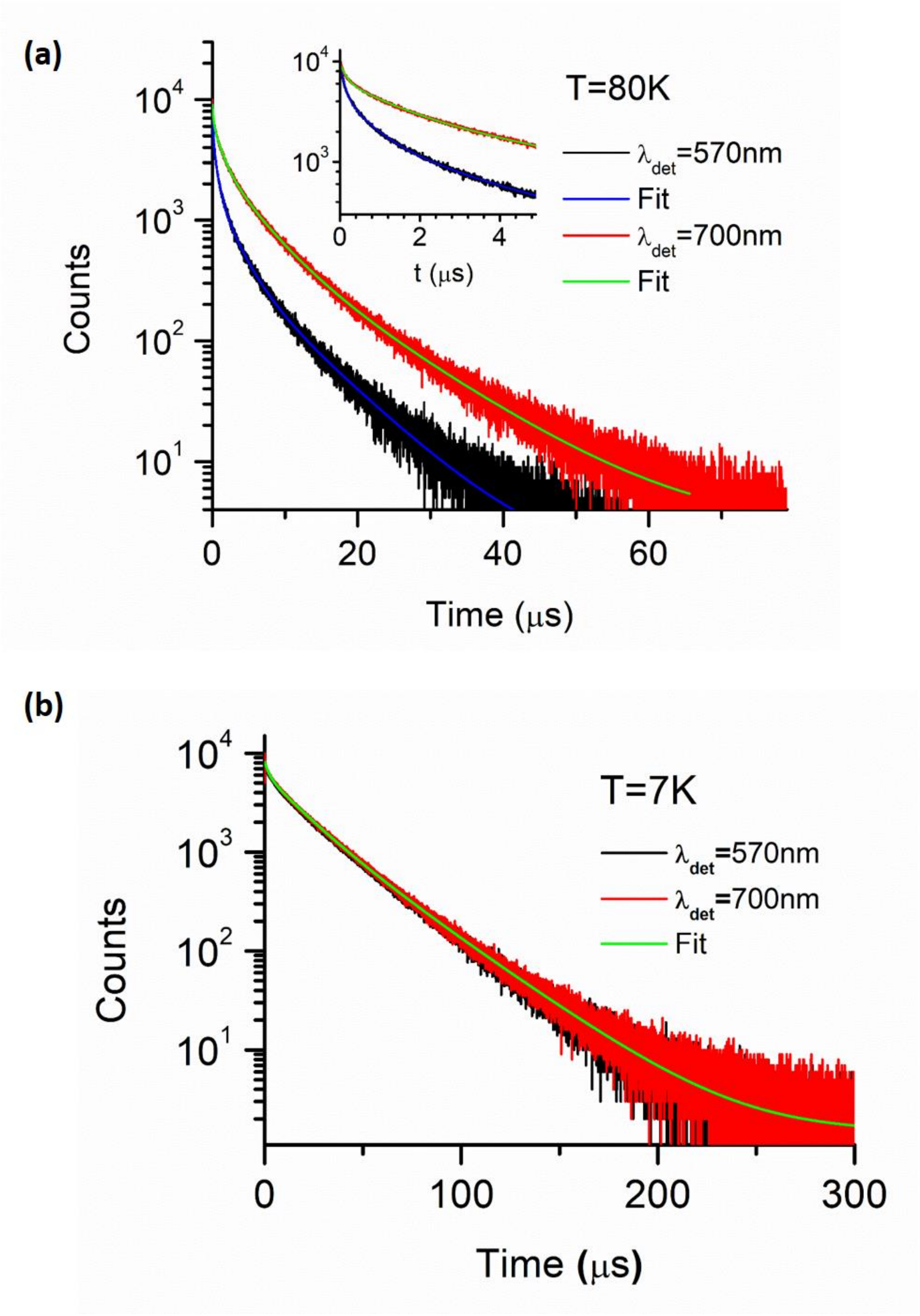

**Figure S13.** Photoluminescence decay at T = 80 K (a) and T = 7 K (b) at different detection wavelengths

## S6. Diffuse reflectance spectroscopy

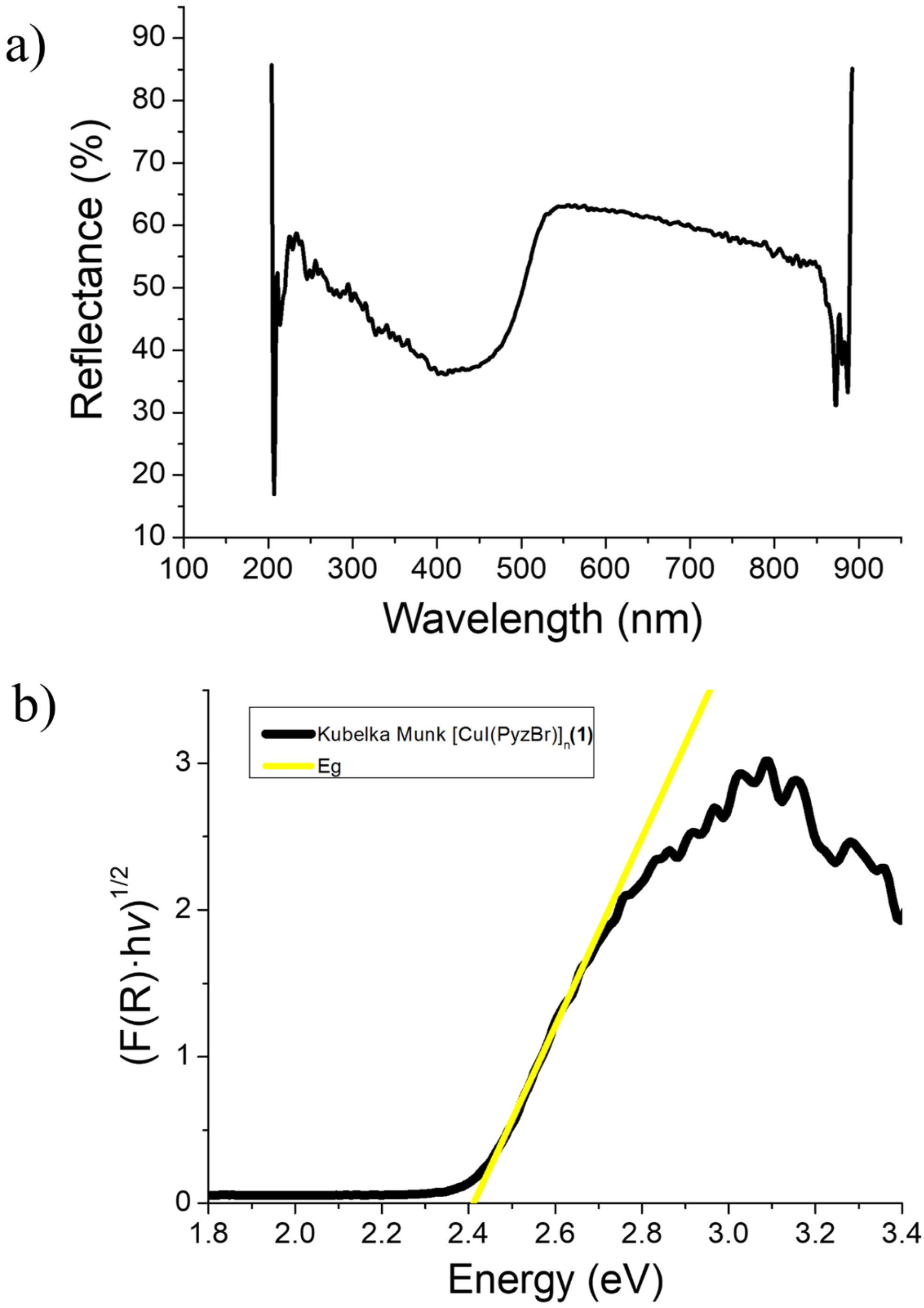

**Figure S14.** Diffuse reflectance spectra in solid state (a) and the Kubelka Munk conversion allows obtaining the gap (b) for compound $[CuI(PyrBr)]_n$ Eg = 2.40 eV.

## S7. Effect of grinding and uniaxial pressure on photoluminescence.

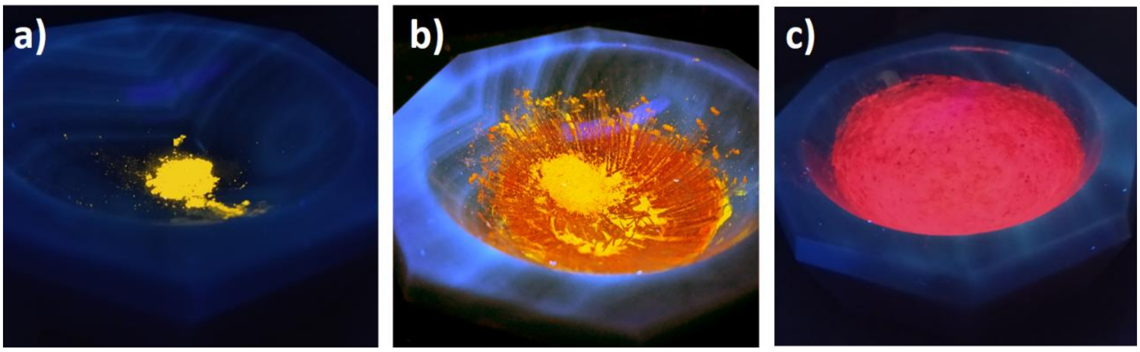

**Figure S15.** Grinding process of **[CuI(PyzBr)]n** (**a**), after 2 minutes of grinding (**b**), and after 10 minutes (**c**) under UV light λ = 365 nm.

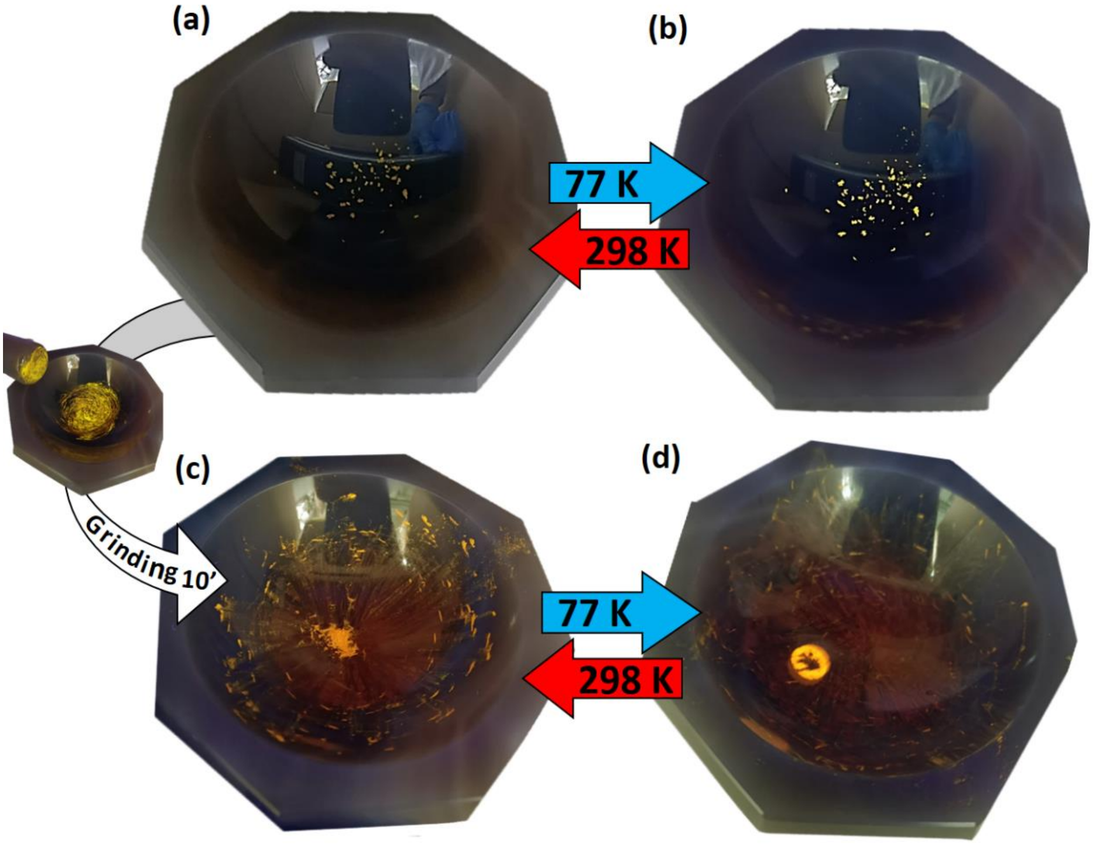

**Figure S16.** Emission from single crystals of **[CuI(PyzBr)]$_n$** at 298K a) and 77K (b) and after 10 minutes of grinding (c and d, respectively)

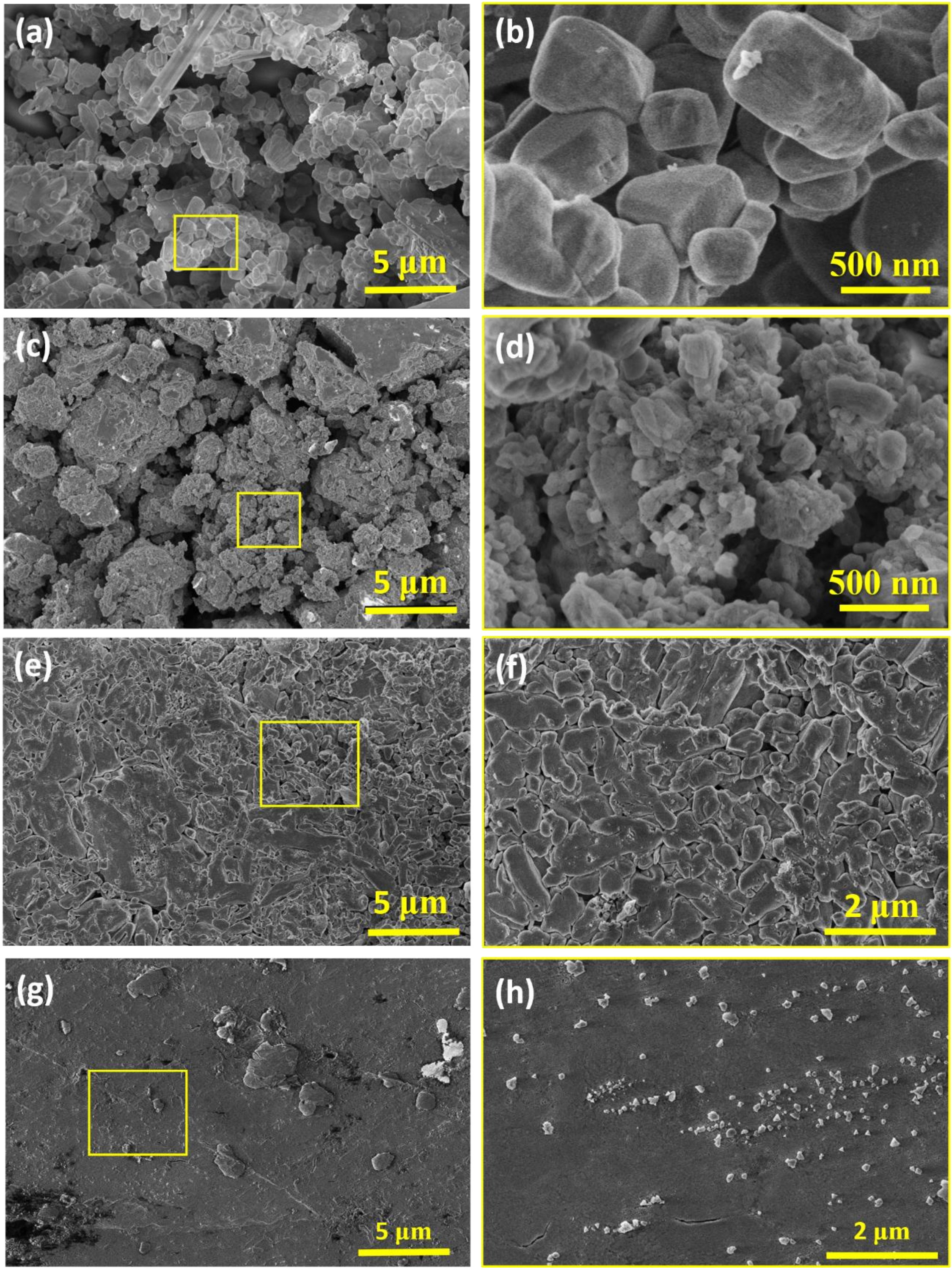

**Figure S17.** Images on the left-hand side: SEM images of **1D-[CuI(PyzBr)]$_n$** after mechanical synthesis (2 minutes grinding) (**a**), after grinding for 10 minutes (**c**), pellet pressed at 1.8 GPa during 10 minutes (**e**) and pellet pressed at 5.5 GPa during 10 minutes (**g**). Images on the right-hand side: zoom into the yellow squares (**b, d, f,** and **h**).

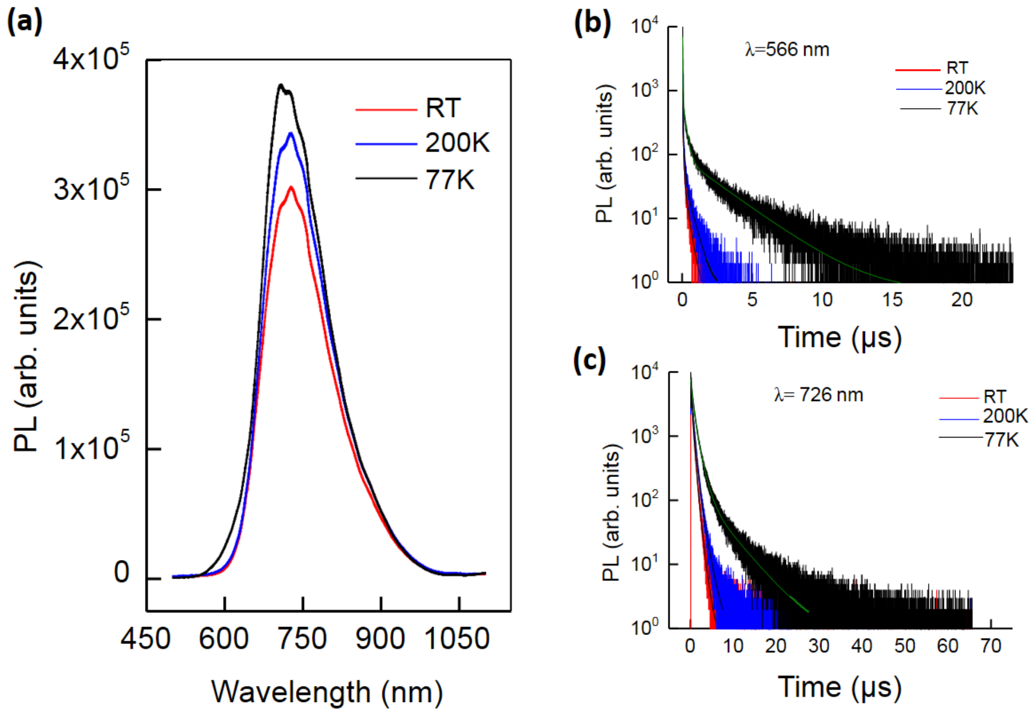

**Figure S18.** Photoluminescence of **[CuI(PyzBr)]$_n$ polycrystals** after 10 minutes of grinding at different temperatures. PL decay curves at different temperatures detected at (**b**) 566 nm and (**c**) 726 nm. The instrumental response function is depicted in red.

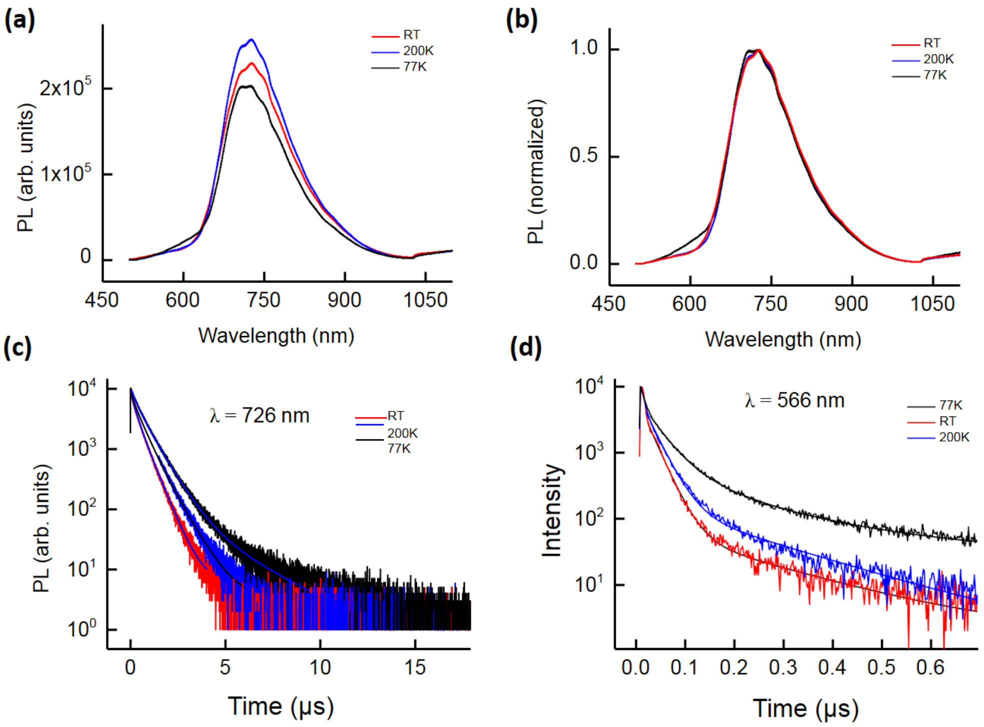

**Figure S19.** Photoluminescence of compound **[CuI(PyzBr)]$_n$ polycrystals** after 10 minutes of application of uniaxial pressure of 3.8 GPa at different temperatures (**a**) and the normalized spectra (**b**). PL decay curves at different temperatures detected at 726 nm (**c**) and 566 nm (**d**). The instrumental response function is depicted in red.

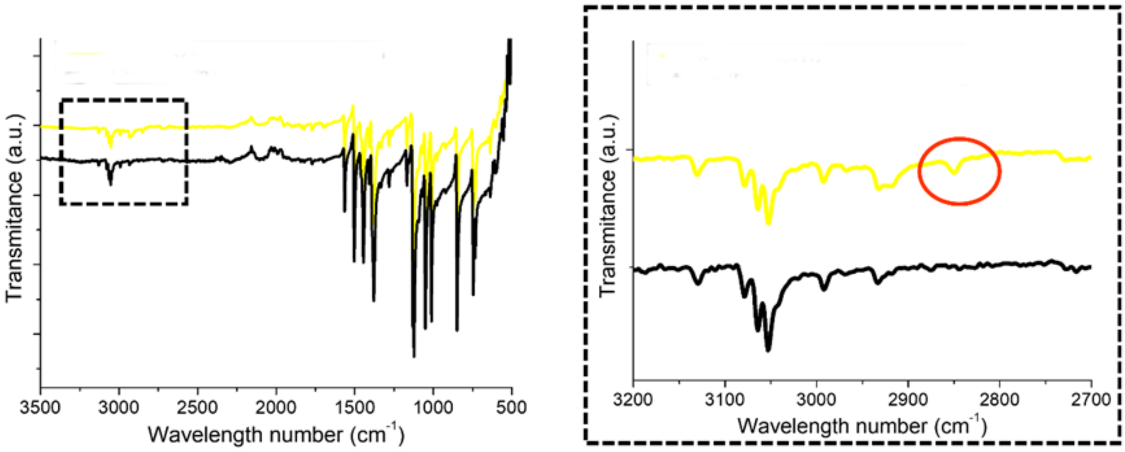

**Figure S20.** IR spectrum and zoom of the spectrum of [CuI(PyzBr)]n (yellow line) and after grinding 10 min in agate mortar (black line). Both spectra coincide in all peaks, confirming that there are no variations in the structure, except for the band encircled in red, which corresponds to the C-H vibration affecting the hydrogen bond and which disappears after grinding

## S8. Effect of quasi-hydrostatic pressure on photoluminescence.

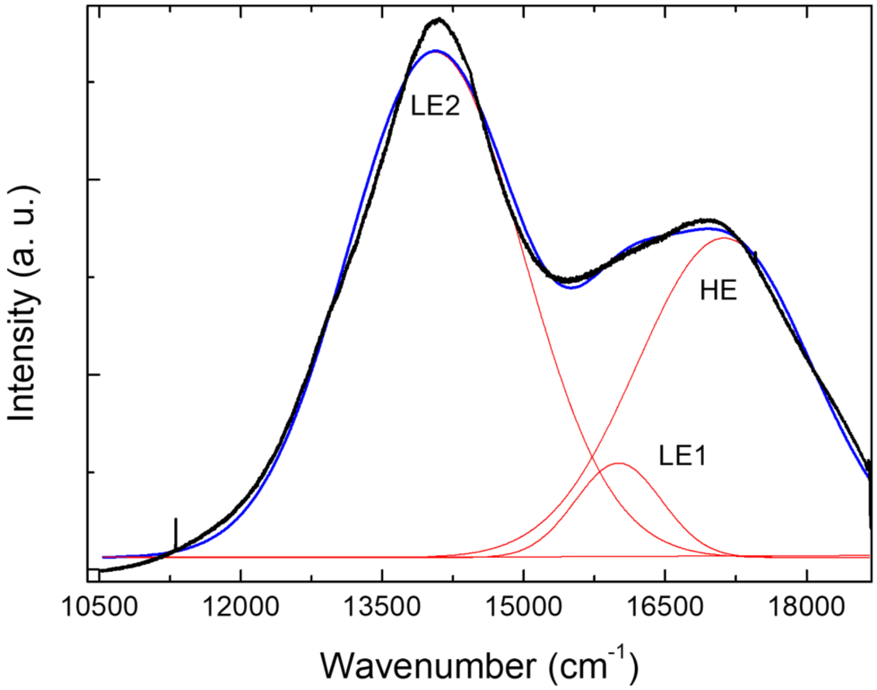

**Figure S21.** Photoluminescence of [**CuI(PyzBr)]$_n$** polycrystals at ambient conditions under 532 nm laser excitation, deconvoluted in three Gaussian components.

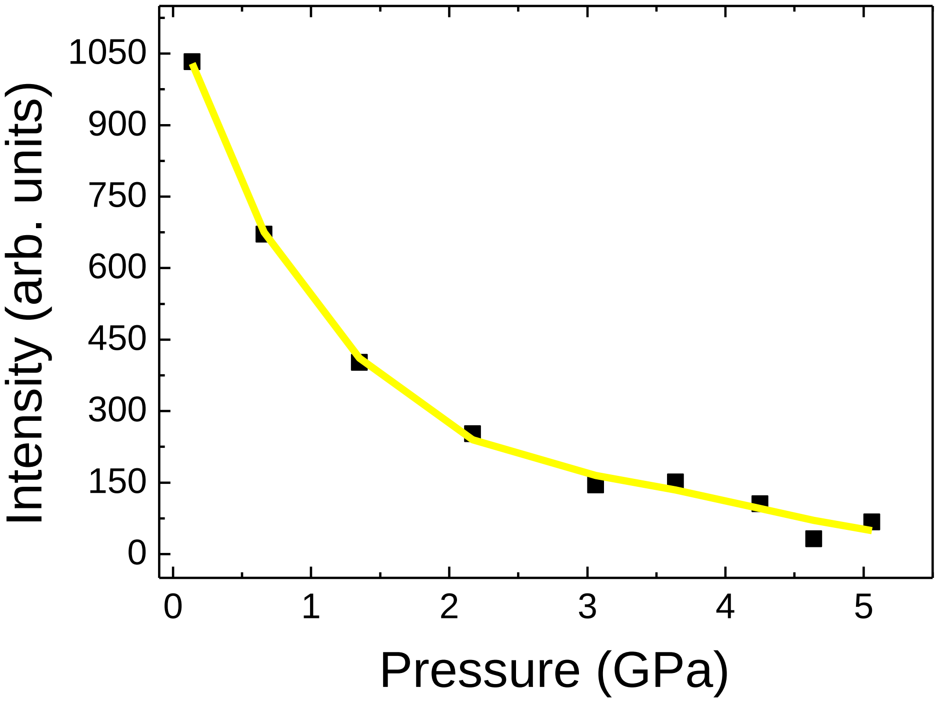

**Figure S22.** Integrated intensity of **1D-[CuI(PyzBr)]$_n$** obtained at 25 °C under 375 nm laser excitation as a function of externally applied hydrostatic pressure.

## S9. Electrical Conductivity

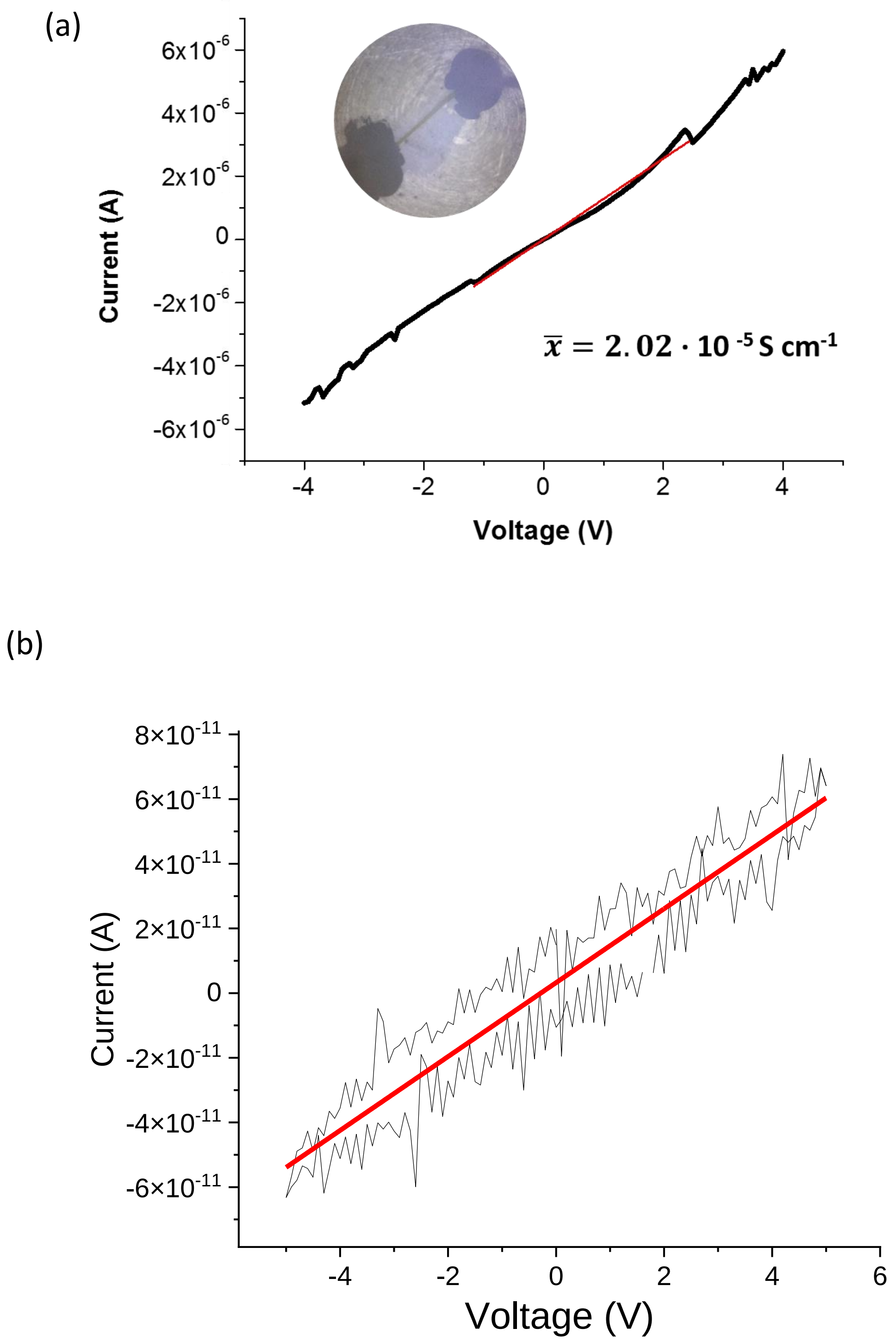

**Figure S23.** Graph of current versus voltage for a **[CuI(PyzBr)]$_n$** single crystal (a) and single crystals pressed into a pellet (3.8 GPa for 10 minutes) (b) at 295 K.

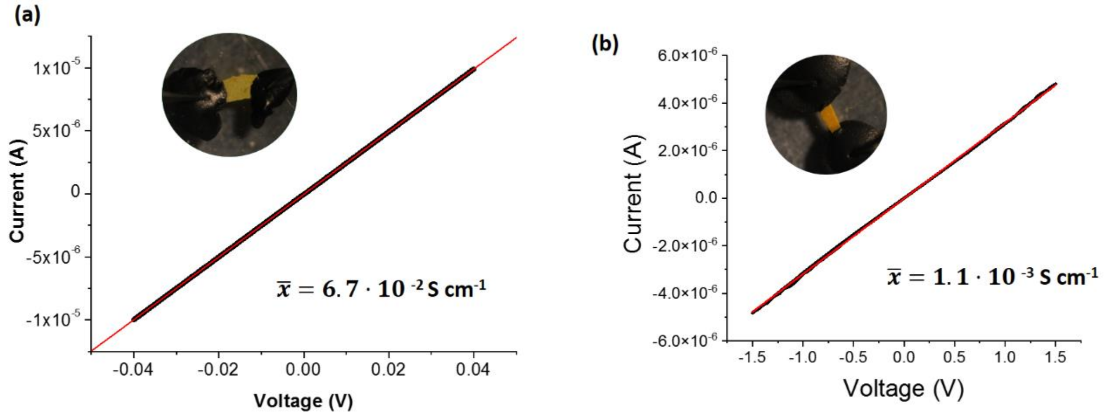

**Figure S24.** Current versus voltage of pellets of **[CuI(PyzBr)]$_n$** polycrystals pressed at 3.8 GPa (a), 5.5 GPa (b) for 10 minutes.

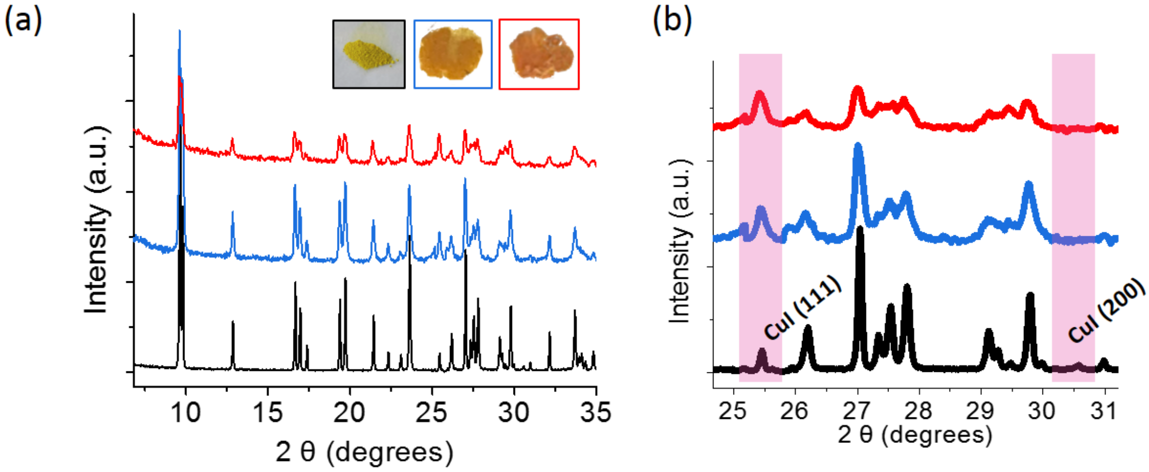

**Figure S25.** PXRD of **[CuI(PyzBr)]n** polycrystalline powder (black line), pellet pressed at 3.8 GPa (blue line) and at 5.5 GPa (red line) (**a**), and the zoom to verify the presence of CuI (b).

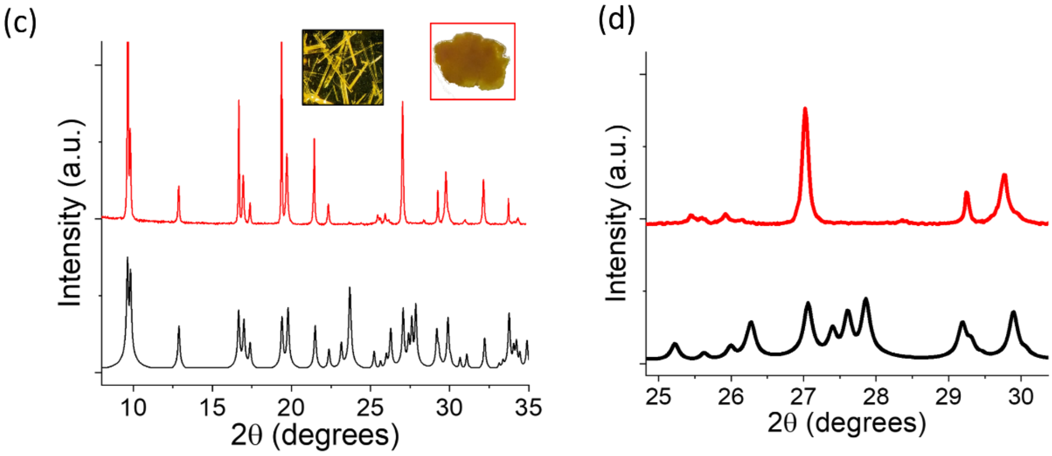

**Figure S26.** PXRD of **[CuI(PyzBr)]n** single crystal (black line), pellet of single crystals pressed at 3.8 GPa (red line) (**a**) and the zoom without presence of CuI (**b**)

## S10. DFT calculations

The computation of the electronic properties of the crystal bulk has been carried out by spin-polarized single point DFT band structure calculations with the Quantum Espresso package.[1] by using atomic coordinates taken from crystal structures determined by XRD at ambient and elevated pressure. The results of the 0 GPa calculation based on a nonmagnetic state (ground-state in both cases), are shown in Figure S27 in the form of a band dispersion diagram over several high-symmetry reciprocal space directions within the first Brillouin zone (with a k-point set of 6×3×2). It is immediately evident that the electronic structure, with a band gap of 0.36 eV at Γ, has a strong band dispersion of the $\varphi_0$ and $\varphi_1$ (quasi-degenerate conduction bands) states (of around ~0.4 eV) from Γ → X (along the metallic skeleton), and virtually none along X → M and Γ → Z vectors, that is, corresponding to interactions transverse to the metallic skeleton axis, which indicates an interesting conducting character along the metallic chain.

Finally, the effect of pressure on the electronic structure is also illustrated in Figure S27, which shows the band structure at 3.8 GPa. The calculation reveals that the electronic nature of the material is preserved under pressure with some symmetry breaking w.r.t. the 0 GPa case; band dispersion from Γ → X increases slightly with compression along the metallic skeleton (~0.5 eV), and the curvature at Γ-point is higher for the 3.8 GPa case indicating a lower effective mass of electrons; but there remains little or no dispersion along X → M and Γ → Z. Although in this case, we observe a wider band gap of 0.54 eV at Γ, a higher dispersion translates into a strong hybridization of the delocalized conducting states, as well as a higher conductance, as evidenced by the experiments.

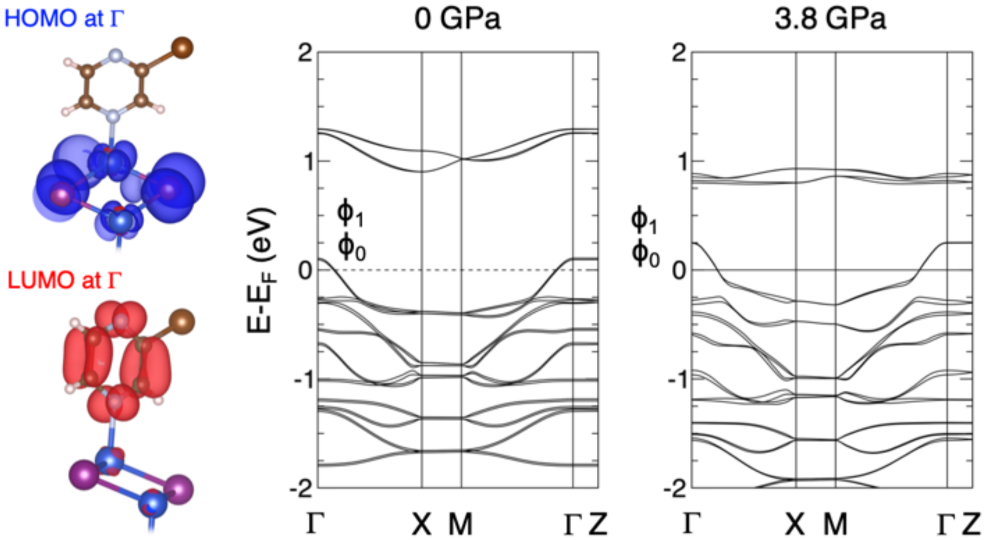

***Figure S27.*** Computed DFT electronic band structure for the crystal bulks at ambient (0 GPa) and elevated (3.8 GPa) pressure. The zero energy is taken to correspond to the Fermi energy, while the *x*-axis labels denote a path through the three-dimensional (3D) space of *k*-vectors. Points of high symmetry in the Brillouin zone are labeled as Γ (0,0,0)→*X*(1/2,0,0)→*M*(1/2,1/2,0)→ Γ (0,0,0)→Z(0,0,1/2), all in reciprocal space coordinates. 3D isosurfaces corresponding to the HOMO and LUMO orbital densities at Γ -point are shown with the same isovalue of 0.001 a.u.

## S11. Bibliography

1. P. Giannozzi, S. Baroni, N. Bonini, M. Calandra, R. Car, C. Cavazzoni, D. Ceresoli, G. L. Chiarotti, M. Cococcioni, I. Dabo, A. Dal Corso, S. de Gironcoli, S. Fabris, G. Fratesi, R. Gebauer, U. Gerstmann, C. Gougoussis, A. Kokalj, M. Lazzeri, L. Martin-Samos, N. Marzari, F. Mauri, R. Mazzarello, S. Paolini, A. Pasquarello, L. Paulatto, C. Sbraccia, S. Scandolo, G. Sclauzero, A. P. Seitsonen, A. Smogunov, P. Umari and R. M. Wentzcovitch, *J. Phys. Cond. Matter.*, 2009, **21**, 395502.